Glyphs for Visualizing Uncertainty in Vector Fields

Craig M. Wittenbrink, *Member, IEEE*, Alex T. Pang, *Member, IEEE*, and Suresh K. Lodha, *Member, IEEE*

Abstract—Environmental data have inherent uncertainty which is often ignored in visualization. Meteorological stations and doppler radars, including their time series averages, have a wealth of uncertainty information that traditional vector visualization methods such as meteorological wind barbs and arrow glyphs simply ignore. We have developed a new vector glyph to visualize uncertainty in winds and ocean currents. Our approach is to include uncertainty in direction and magnitude, as well as the mean direction and length, in vector glyph plots. Our glyph shows the variation in uncertainty, and provides fair comparisons of data from instruments, models, and time averages of varying certainty. We also define visualizations that incorporate uncertainty in an unambiguous manner as verity visualization. We use both quantitative and qualitative methods to compare our glyphs to traditional ones. Subjective comparison tests with experts are provided, as well as objective tests, where the information density of our new glyphs and traditional glyphs are compared. The design of the glyph and numerous examples using environmental data are given. We show enhanced visualizations, data together with their uncertainty information, that may improve understanding of environmental vector field data quality.

Index Terms—Verity visualization, wind profilers, doppler radar, wind barbs, icons.

1 Introduction

VISUALIZATION graphically displays large amounts of data to give us a better understanding. Generally, data have associated characterizations of quality or *uncertainty*. While the uncertainty is an essential part of the data, it has often been ignored while processing or displaying. There is a need to display the original data together with their uncertainty for accurate interpretation. Integrating data quality into visualization is an important challenge to make visualization a more effective tool. We answer several important questions in visualizing the uncertainty in environmental vector fields, including: How are different forms of uncertainty represented in vector fields? How are inaccuracies introduced in interpolations used in vector field visualization techniques? How can we visualize vector field uncertainty? And, how can we combine or multiplex uncertainty into standard vector field visualizations to improve understanding?

In a one dimensional data plot, such as a time series scalar plot, the uncertainty can be graphically represented with a glyph that shows the median, quartile, minimum, and maximum values. Two examples of such glyphs are Tukey's box plot [39] and Tufte's quartile plots [37]. These glyphs can graphically present a sample point's distribution efficiently. When going to higher dimensional data, or higher densities of data, the box plot becomes unwieldy.

This paper is focused on different ways of mapping uncertainty parameters to visual cues in vector field visualization. The challenging and novel aspects of this research are the integration of the data and its uncertainty for an accurate depiction; and the generalization of vector visualization methods to include uncertainty.

Our visualization work involves atmospheric and oceanographic data [22], [27], [28], [29]. We show two techniques for visualizing uncertainty, the overloading approach (color, transparency, etc.) and new glyphs which do not require overloading. We call this nonoverloading approach *verity visualization*. Verity visualization is not always possible, but is a significant improvement because it leaves overloading for other variables.

The effectiveness of our glyphs is measured both by quantitative and qualitative measurements. Quantitative metrics include Tufte's principles of data-ink maximization [37], information per unit of space, information per unit of ink (number of colors), number of multifunctioning graphical elements, and the data density for the entire graphic. These methods are used to objectively evaluate the effectiveness of placing larger and larger amounts of data into a visualization with economy of expression. Additional metrics include those suggested by Kosslyn [16] who breaks graphs into four structural components. One of these qualitative components is the specifier, a graphics attribute such as length. The other components are frameworks, labels, and background. Cleveland et al. [5], [6] use specifiers as the groundwork of a theory of graphical perception. We evaluated specifiers in our graphics by using application specialists, through our collaboration with the Department of Meteorology at the Naval Postgraduate School, Monterey, California. We have done a perceptual survey to evaluate our verity visualization techniques. This user evaluation provides important feedback and indicates general trends in the effectiveness of our uncertainty visualizations. In addition, our uncertainty glyphs for environmental data may generalize to other scientific data.

• *The authors are with the Baskin Center for Computer Engineering & Computer Science, Applied Sciences Building, University of California, Santa Cruz, Santa Cruz, CA 95064. E-mail: craig@cse.ucsc.edu.*

For information on obtaining reprints of this article, please send e-mail to: transvcg@computer.org, and reference IEEECS Log NumberV96021.

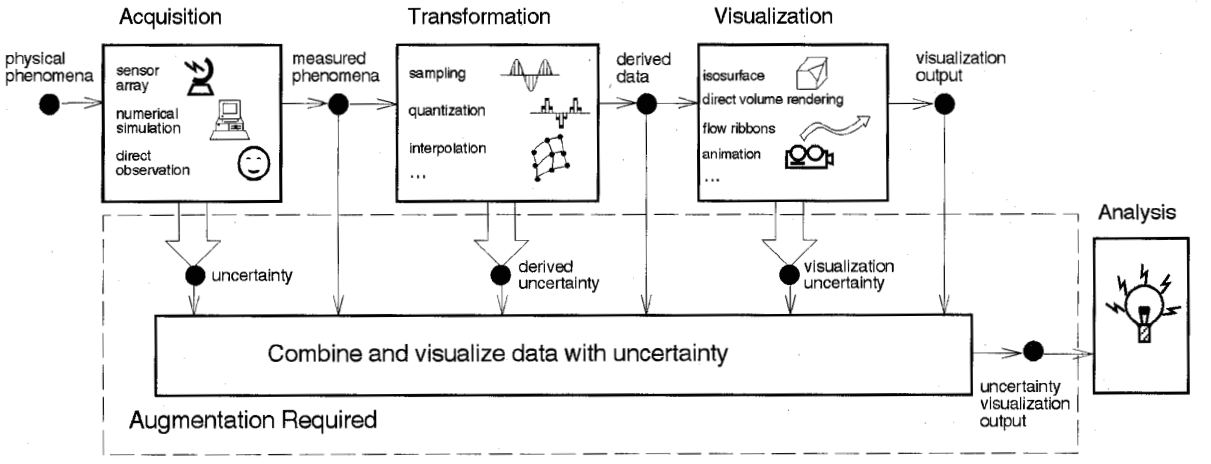

Fig. 1. This augmented visualization pipeline shows measurement uncertainty, derived uncertainty, and visualization uncertainty. Our glyphs attempt to multiplex these uncertainties with the data sources from the visualization pipeline.

Visualization that does not properly represent uncertainty is unreliable and misleading. Combined data and uncertainty visualization allows more precise interpretation. Scientific visualizations with combined uncertainty may also be shown to be superior with quantitative metrics, and qualitative tests can evaluate user interpretation. Visualizing uncertainty will significantly improve understanding of environmental phenomena. Section 2 defines uncertainty, enumerates previous work, and defines our methodology for evaluating uncertainty along each step of the visualization pipeline. Section 3 presents our new uncertainty visualization vector glyphs. Section 3 also defines verity visualization, contrasts it with data overloading, and defines the uncertainty vector glyph's design. Section 4 gives results of both quantitative and qualitative evaluation. Section 5 concludes the paper.

2 Methodology and Background

Many definitions of uncertainty have been proposed [1], [13], [24], [36]. Uncertainty is a multifaceted characterization of data (value, range/domain-time, and space) that encompasses many concepts including: error, inaccuracy, validity, quality, lineage, statistical variability, and scientific judgment. There has also been a great deal of work on glyphs for mapping multiple variables.

2.1 Defining Uncertainty

Error can be defined as the discrepancy between a given value and its true value [13]. Inaccuracy is the difference between the given value and its modeled or simulated value [13]. Data validity encompasses both the inaccuracy of the data and the procedures applied to the data. Data validity is measured by deductive estimates, inferential evidence, data consistency and comparison between independent sources, and it is ratified by testing [13], [24]. Data quality is treated as an even more general term that includes data validity and data lineage. Data lineage refers to those characteristics of data such as collection circumstances and pedigree. Data quality can be defined as a three parameter variable that consists of goodness or statistical measure, application or model resolution, and purpose such as analysis or communication [1]. Due to the importance of the presence of uncertainty in scientific data, National Institute of Standards and Technology [36] has recently formulated guidelines for expressing uncertainty of data measurements. Data uncertainty, although consisting of several components, can be broadly classified into two categories according to the method used to estimate their numerical values: evaluation by statistical methods such as standard deviation or least squares, and evaluation by scientific judgement. The National Center for Geographic Information and Analysis initiative on "Visualizing the Quality of Spatial Information" [1] classifies the sources of data uncertainty as source errors, process errors, and use errors.

2.2 Data Sources

Our work on the REINAS project (Real-time Environmental Information Network and Analysis System) [21], [22] has uncovered challenges in dealing with uncertainty from both instrument and numerical model data. The data that we investigated are from instruments, numerical models, and interpolation. Instrument data sources include radars that measure wind [17], [19] or ocean surface currents, meteorological stations (wind, pressure, temperature, and humidity), and sonar buoys (currents). We have access to output from numerical models such as the Navy Operational Regional Atmospheric Prediction System (NORAPS) [14] and the Princeton Mellor Model [23]. The quality of these data depend on the simplifying assumptions that were made in creating the model, numerical accuracy, spatial and temporal resolutions, and initial and boundary conditions. Typically, the meteorological station and buoy data are sparsely sampled and contain fixed uncertainties, while the radars and circulation models produce denser, gridded outputs with varying uncertainties. The interpolated data are derived from the measured and simulated fields.

2.3 Data Uncertainties

Although advances have been made in defining and deriving uncertainty for data collected from instruments, the identification of the occurrence of uncertainty and its distribution in the visualization pipeline is crucial in identifying the effect of uncertainty on data interpretation. To illustrate the different sources of error that arise from the transformations that are applied from data collection

through visualization, Fig. 1 shows a data pipeline starting with the data *acquisition* where the physical phenomena are captured and recorded either through sensors or as output from numerical models. These measured phenomena may undergo *transformations* to produce derived data. The derived data are processed by *visualization* algorithms that generate images for the users to *analyze*.

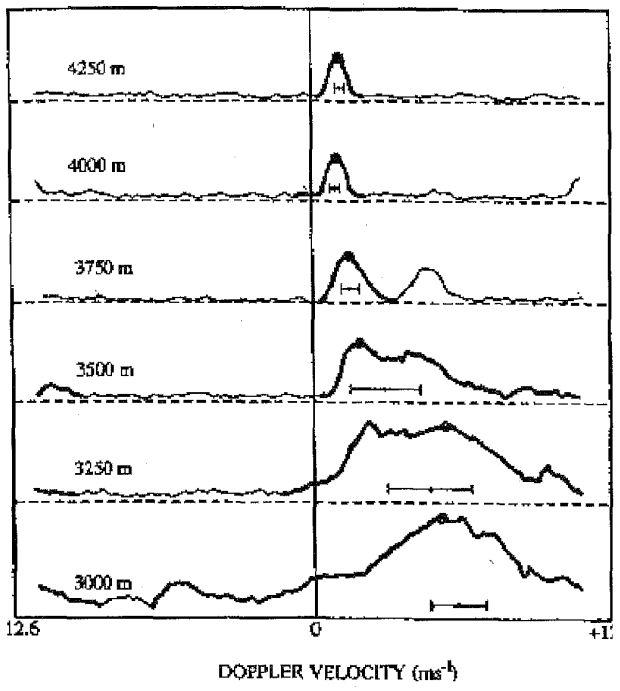

Fig. 2. Spectral samples of wind velocity from a vertical wind profiler. The plot for each height level shows the frequency versus magnitude of signal return. Lower elevation returns show wider spreads indicating contamination from migrating birds and higher uncertainty (from [40], Fig. 5).

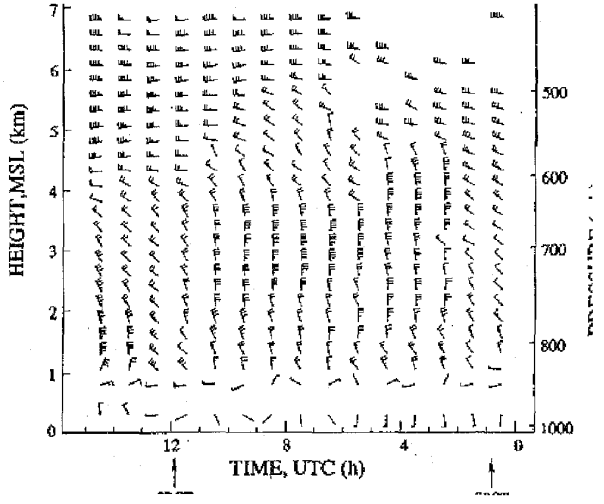

Fig. 3. Time vs. height display of hourly consensus-averaged wind using wind barb glyphs (from [40], Fig. 9).

Fig. 1 shows where uncertainties are introduced in the data pipeline. Data uncertainties are introduced and propagated at every stage in the pipeline. Measurement errors result from equipment limitations, miscalibration, and environmental effects. Model errors result from model simplification, initial and boundary conditions sensitivity, and numerical imprecision. Transformation errors result from approximations and numerical imprecision. Visualization errors result from similar effects in visualization software. Fig. 1 shows the augmentation of the data pipeline to deal with uncertainty. Uncertainty may be introduced during the acquisition (uncertainty), transformation (derived uncertainty), and visualization (visualization uncertainty). In this paper we focus on, and give examples of acquisition, model, and interpolation uncertainties. Uncertainty for measured data are provided by instruments [17], [40] or from the estimated accuracy of the instrument [4]. As an example, the wind profiler [40] measures wind velocity in three directions by sending out three beams. The radar outputs statistical information, including the signal to noise ratio, width of the radar signal return beam, and the maximum strength of the signal. These features are shown in the example radar spectral returns in Fig. 2. The radar uses thousands of samples from the same beam over a minute to create minute averages that are used to compute a consensus of returns over ten minutes or an hour. The radar calculates spectra for many heights as shown in Fig. 2. We use the distribution, standard deviation, mean, minimum, and maximum as components of uncertainty for each beam's radial velocity. Three radial velocities are then used to calculate the planar wind velocity, and the magnitude and directional uncertainty. Fig. 3 shows wind barbs to visualize winds measured by a wind profiler at different heights, and consensus averages at 15 separate hours. No uncertainty information is encoded. The wind barbs, as do the wind glyphs throughout this paper, have their endpoints at the datapoint, an environmental data convention. Winds are also defined only in the two-dimensional plane above the earth, and have no vertical component. The flag denotes the wind strength each short flag representing a 5-knot increment and each longer flag a 10-knot increment.

As another example, the data collected by meteorological stations do not have any indication of uncertainty for each data point, other than an expected accuracy of the sensors. However, similar to the wind profiler processing, time averages and statistics are used to calculate the distribution of measurements over a longer time interval than the base sampling rate. From this distribution, the standard deviation, mean, minimum, and maximum are computed giving uncertainty for time averaged data. This approach is especially useful when there is a high density of stations as in the test networks described in Clark et al. [4], because you have correlated stations for comparison.

For model data, the uncertainty is obtained by multiple, runs of the model, either with different starting conditions, with different grid spacings, or with comparison to measurements as done by Clancy et al. [3]. The radar data can be combined between sites using a maximum likelihood algorithm, that also calculates uncertainty. Specifically, Codar Systems Inc. radars (SeaSonde (TM)) [20], [22] are now in-

stalled in three positions around Monterey Bay so that their look directions intersect and provide three measurements of the ocean surface current. The best ocean surface currents are those that are measured at orthogonal directions from at least two sites, but the nearly nonorthogonal sites may also be useful if sufficient uncertainty information is provided.

The sparseness of much of the environmental data requires interpolation and extrapolation to assist scientists in visualizing the effects of environmental phenomena. Interpolated data provide a derived uncertainty from the measured data, and in many cases are acceptable to use for scientific visualization. Our early work focused on interpolation uncertainty using weighted interpolation from sparse meteorological stations [29]. We have done some work to characterize the interpolation effect on data visualization, using a linear falloff assumption. (See Example 3 in Section 3.3.) During visualization, the representation of uncertainty is followed by the challenging task of mapping uncertainty to visual cues. The task is complicated for several reasons. First, which aspect of the different parameters that constitute uncertainty is to be visualized? Second, which visualization primitives and rendering algorithms are to be utilized? These steps may introduce their own sources of errors. Compounding the problem, the errors at each stage may propagate and influence succeeding stages in the data pipeline. Identifying the sources of uncertainty and their distributions is critical in assisting scientists to analyze their data accurately.

2.4 Previous Work

Most of the work in visualization of data with uncertainty is in the field of Geographic Information Systems (GIS). See, for example, the survey of methods in Hunter et al. [15]. Little work in visualization of data uncertainty has been pursued in other areas, and we briefly survey techniques below. For the following, we define glyphs as symbols that represent data through visual properties such as color, shape, size, and orientation. Specific examples of glyphs are vector arrows and wind barbs. Glyphs are also called probes, geometrical primitives, stars, boxes, and icons. We prefer the term glyphs because icons refers to data symbols, images, and graphical elements representing concepts, objects, or actions within a user interface. The terminology is not well defined or standardized [32], and other researchers do use icon, such as Grinstein et al. [31], [35], and Post et al. [33]. Glyph has been used with less ambiguity in the graphics and visualization literature.

Glyphs are used to represent univariate data in Tukey [39], Tufte [37], [38], and Cleveland [5]. Glyphs can also represent multivariate data as shown by Cluff et al.'s survey [7] of stars, Chernoff faces, boxes, profiles, Kleiner-Hartigan trees, and Andrew's plots. More recent glyphs or probe techniques for vector and tensor fields are shown in de Leeuw et al. [8]. There have also been systems designed for tailoring glyphs to data such as Ribarsky et al.'s Glyphmaker [34]. Displacement vectors can be used to display differences or errors between two images such as in Peterson [30]. However, we have only recently found glyphs, distinct from our own, used to display uncertainty information in vector fields [33].

An approach to visualizing uncertainty is to map it to different graphics attributes. Uncertainty can be seen as additional variables which are input to properties of the graphic. This can be done with the multivariate glyphs just mentioned. Graphics attributes include: color, transparency, and line width. Thus, examples that fall under this category include: varying contour widths depending on certainty [9], mapping uncertainty parameters to different points in HSV space [18], using cross hatches [25], and our work in using transparency to indicate confidence in an interpolated field [29] to name a few. Most of the previous work on visualizing uncertainty is focused under this category.

Other graphics and rendering techniques may be used for visualizing uncertainty. Methods include overlaying (sandwich layers) or side-by-side comparisons of data and uncertainty information (Wills et al. [41]) pseudocoloring of difference and error images such as our volume rendering comparisons [42], haziness corresponding to uncertainty (Beard et al. [1]) and defocusing or Monte Carlo blurring (Fisher [10]). Animation by playing back sequenced images (Monmonier [26]), random dots (Fisher [11]), and segmenting and blurring (Gershon [12]) have been used to display data uncertainty. Even sonification has been proposed by Fisher [11] for perceiving uncertainty. Our glyphs typify a new class of technique we call *verity visualization*.

3 Results

Our research on visualizing uncertainty in environmental vector fields is organized into four parts: collecting and characterizing different data, defining and deriving uncertainties, visualizing data with uncertainties, and evaluating the new visualization methods. The primary focus of the paper is on creating new visualizations for data with uncertainties (Sections 3.1 to 3.3). This requires computing the uncertainty for the data, which we discussed briefly in Section 2.3.

3.1 Visualizing Data with Uncertainty

In order to contrast our new visualizations with existing methods, we first describe overloading for visualizing uncertainty by mapping uncertainties to additional visualization parameters. With overloading the user may still be able to confuse the overloaded graphics specifier and what data are mapped to it. As an example of overloading, consider visualizing a surface with the uncertainty of the surface controlling the color. Such a pseudocoloring approach works with many visualizations including contours—color contours, glyphs—colored glyphs, etc.

At the other extreme, we have also found that instead of treating uncertainty as an additional piece of data, the uncertainty information is integrated with the data into the visualization graphic so that users cannot help but interpret the resulting image holistically. We call this *verity visualization*—in that it *suggests the quality of the data that is exactly what it purports to be or is in complete accord with the facts.* It should be noted that treating uncertainty information as additional data to be visualized or treating them through verity visualization is a continuum rather than a distinct dividing line in some instances.

The wind vector can be denoted in a visualization with a glyph, a symbol indicating the strength and direction of the wind. In meteorology, wind barb glyphs, as shown in Fig. 3, are used to encode the bearing and magnitude. In

many visualization tools, the glyphs are simply arrows whose lengths are scaled to the vector magnitude. There are several options available to indicate uncertainty associated with the wind vector. The most obvious is to overload the graphics attributes of the wind barbs, for example, with pseudocoloring and transparency. Alternatively, uncertainty may be shown with an underlying color map. Shading, transparency, and uncertainty contours may all be used if uncertainty is viewed as another datum to be plotted. However, the resulting images still require a separation of interpretation between the graphics attributes. One also loses the flexibility of using those shadings, transparencies, or contours to display other variables such as temperature or pressure together with the wind field. We have worked out a new glyph design that encodes magnitude, and bearing uncertainty, as well as bearing and magnitude that we describe in the next section. Following that section, we present some examples of using our glyph with environmental data to demonstrate the broad applicability of the glyph.

3.2 Glyph Design

There are an infinite number of variations in glyph design. The designs that we have developed focus on the ability to clearly display uncertainty in magnitude and direction. The evaluation of a glyph's effectiveness must address dense displays. A glyph which is apparently quite effective in isolation does not necessarily work well in a dense plot. This perceptual element in glyph design can also be extended to graphics attributes. For example, line or surface thickness can be mapped to uncertainty levels. However, thicker or bolder lines also stand out more visually and tend to emphasize rather than de-emphasize fuzzy areas of the data as shown by the length scaled glyphs in Fig. 10 compared to Fig. 11. On the other hand, thicker lines or surfaces may be counterbalanced by lowering the brightness level. Likewise, textures can also depict areas of uncertainty, but we group these effects into the overloading approach.

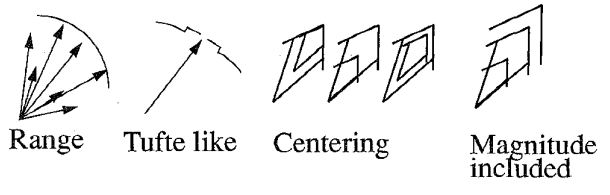

Fig. 4. Glyph design.

Fig. 5 shows a variety of possible glyphs to encode uncertainty. Whether glyphs encode uncertainty in magnitude or angle (Fig. 4) or both is indicated in the columns. The bearing uncertainty is shown with a loop around the arrow head, pie swept area, ellipsoidal target area, etc. The magnitude uncertainty is also shown by the loop (Fig. 5, row one), encoded in the body of the consumer reports-like glyph (row three), by the range of the pie swept area (last row, first column), or by multiple arrow heads (last row, fifth column). While each glyph looks promising in isolation, placing them into a large field gives different results. Figs. 4 and 5 are included to record the alternatives we considered before settling on the glyph used for the visualization and evaluation, Fig. 7. The chosen glyph provides both a clearer indication of flow and uncertainties than the alternatives. For example, the Fig. 4 Tufte-like glyph actually appears to flow backwards when placed into a high density field. We have also investigated the ability of the glyphs to encode uncertainty in different coordinate frames. It is important to have a single coordinate frame for uncertainty which subsumes all other possible coordinate frames; this means that the uncertainty has no secondary effects from the basis used to represent them. Since the (x, y) breakdown is coordinate space dependent, our vector uncertainties and glyphs represent the uncertainties in deviation in bearing and deviation in magnitude. Fig. 6 shows that uncertainty in directions x and y (dx, dy) can be converted to uncertainties in magnitude and bearing.

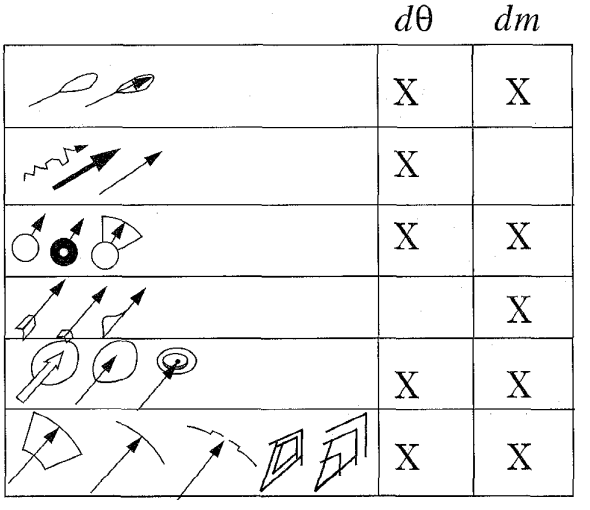

Fig. 5. Variety of glyphs considered for magnitude and angular uncertainty.

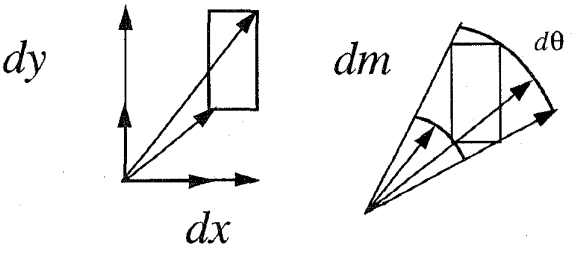

Fig. 6. Glyph coordinate issues.

There are two ways to draw our most promising glyph: one, using the glyph area as magnitude, or, two, using the glyph length as magnitude. The uncertainty glyph can be drawn by connecting vertices 0, 1, 2, 3, 4, 5, and 0 in a counterclockwise order as shown in Fig. 7. The glyph body coordinates to solve for are the main body length l_b, the arrow head length, l_a, the height from the baseline, h, and the winglets of the arrowhead. The uncertainty glyphs are wide arrows that indicate bearing and magnitude. The width of the arrow heads indicate the range of possible bearings at that location. Extra arrow heads indicate the range of possible magnitudes, as shown in Fig. 4 with magnitude included.

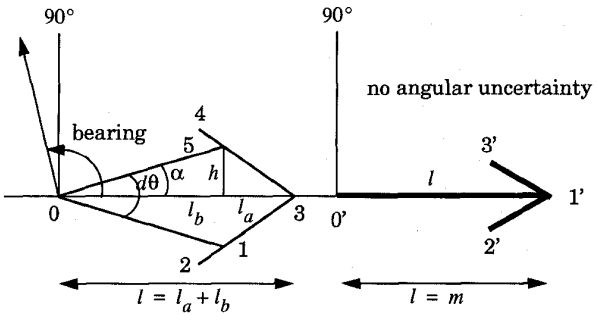

Fig. 7. Glyph parameters.

The parameters that are given are the magnitude, m, the ratio of the head to the body, $r_{a/b} = l_a/l_b$ (or a fixed size of the head l_{head}), the bearing uncertainty, $d\theta$, and the magnitude uncertainty, dm. Using the total length as $l = l_a + l_b$, $\alpha = d\theta/2$, and mapping the magnitude to the area, $m = l * h$. We solve for the body length via trigonometry,

$$l_b = \sqrt{m / (\tan\alpha * (r_{a/b} + 1))}.$$

The other parameters are then solved for using l_b:

$$l_a = r_{a/b} * l_b,\ h = m/l_a + l_b,\ wing_{dx} = r_{a/b} * l_a,$$

and $wing_{dy} = r_{a/b} * h$.

When the length is proportional to the magnitude, we set $l = m$, and solve for $l_b = m/(r_{a/b} + 1)$, $l_a = m - l_b$, and $h = l_b \tan\alpha$. So the winglets of the glyph may be drawn in the same proportion that the head is drawn to the body of the glyph, or constant for all glyphs. These same solutions are used for the three magnitudes m, and $m \pm dm/2$. For the lower deviation and upper deviation, only the front edge of the arrow is drawn, Fig. 4 far right, and Fig. 5 bottom row.

When using a mapping of magnitude to area, there is a limit in the narrowness of the glyph which makes sense, and that relates to the area of the displayed pixels used in the plot. For example as the angular uncertainty narrows down, one might think that the glyph would run off to infinity. But, because any line drawn has a finite width in pixels, it has an area. We solve this by computing the glyph in a pixel grid, and then converting coordinates to world space. In this way, the exact area covered by pixels is known, and glyphs can be drawn as simple arrow glyphs when the angular uncertainty would be narrower than the width of a pixel. This is important as the glyph's approximation should change when it is no longer different than a certain glyph (zero uncertainty glyph).

There are some caveats about plotting any glyph, and we quickly cover some of them here. When the magnitude is effectively zero, we plot a point to indicate that there was a data point with no magnitude, and no arrow head is plotted.

When the uncertainty is greater than 180 degrees in spread, the glyph of a half or more disk is used. The design of the arrow heads is another free parameter for both arrow and uncertainty glyphs. We found users prefer the arrow heads to keep a constant size irrespective of the magnitude, and that narrower tips are preferred to wider ones. When the magnitude $m - dm/2$ is negative, a lower deviation is not drawn.

3.3 Environmental Vector Field Examples

The following four examples illustrate the difference between overloading and verity visualization.

EXAMPLE 1. *(Overloading Approach of Radar Sensed Currents)* Codar ocean surface current radars measure back scattering from the ocean surface and use the doppler shift to calculate the speed that waves are travelling towards or away from the radar. Radial speeds from two or more radars can be combined to generate derived ocean surface currents. The Codar fields shown in this paper are from November 24, 1994, 00:00 GMT, and were collected in Monterey Bay, California, using a radar at the North end of the bay and one at the South end of the bay. Fig. 8 shows a simple example of pseudocoloring the arrow glyphs to the magnitude uncertainty, and pseudocoloring the ocean surface to the bearing uncertainty of the surface current. Fig. 8 was generated by our Spray rendering software [27]. This overloading gives the viewer complete knowledge of the uncertainty, but additional variables cannot be mapped to color. This example uses two different color maps to encode the uncertainty. Users are forced to decode the uncertainty information separately from the currents.

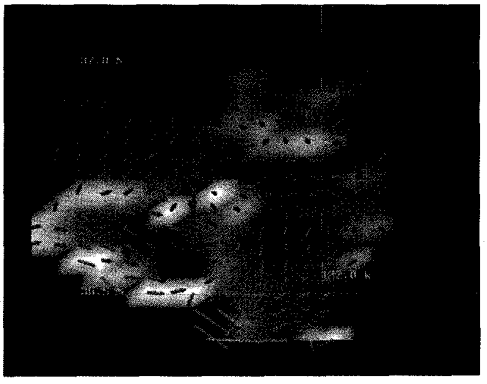

Fig. 8. Ocean currents in Monterey Bay are shown with arrow glyphs whose colors are mapped to the magnitude uncertainty. Angular uncertainty of the current field is mapped from black to white. This figure was generated from Spray [27].

EXAMPLE 2. *(Verity Visualization Approach of Radar Sensed Currents)* To illustrate the point that uncertainty be treated through verity visualization, we apply the new glyph. Fig. 16 shows uncertainty glyphs that encode all of the data visualized in Fig. 8. Different methods for combining radial currents may be used with varying results. We show them to compare the utility of the glyph in different densities of fields, and with different ranges of uncertainty. In Figs. 9, 10, 11, 12, 13, 14, 15, and 16, we show two methods (Method I and Method II) for combining radials from two sites, with the same radial data. Figs. 9, 10, and 11 visualize the same ocean current data derived by Method I using three different glyph types. Figs. 12, 13, 14, 15, and 16 visualize the ocean current data derived by Method II. Figs. 15 and 16 are simply enlarged ver-

sions of Figs. 12 and 14. Codar vector calculation Methods I and II [20] use different averaging areas, so the plots with more vectors are more heavily averaged showing that the user must understand the origin of the data as Method II looks better but may not be any more accurate.

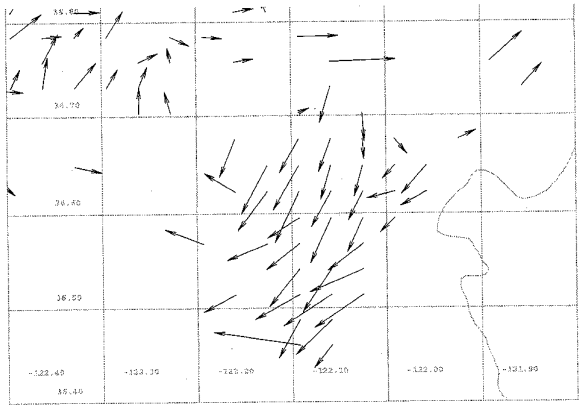

Fig. 9. Arrow glyphs, length scaled to magnitude, codar vector calculation Method I, Wednesday Nov 24 1994.

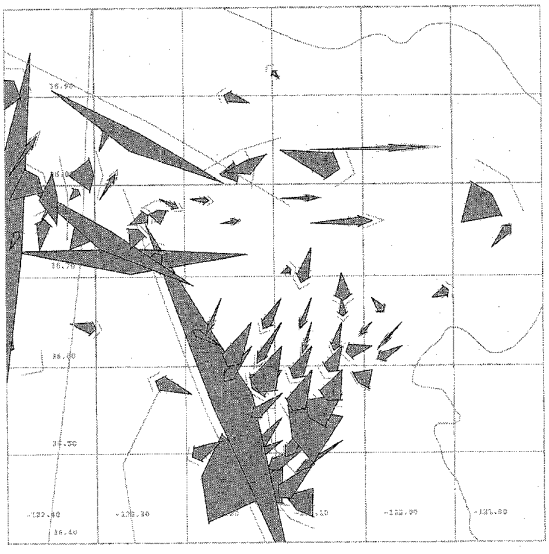

Fig. 10. Uncertainty glyphs, length scaled to magnitude, codar vector calculation Method I.

The sparse current vector field in Figs. 9, 10, and 11 (Method I) is helpful in describing the utility of the new glyph. In Fig. 9, no uncertainty is indicated, and we must take each arrow as equally valid. In Fig. 10, the highly uncertain vectors are very wide showing that many of the measurements have from 20 to 160 degrees of angular uncertainty, and appreciable magnitude uncertainty shown by the upper deviation arrow heads. The glyphs in Fig. 10 have the same length as those in Fig. 9. Highly uncertain measurements are very large which could be perceived as magnitude [37]. Fig. 11 shows uncertainty glyphs whose areas are proportional to the magnitude. This greatly reduces the size of the uncertain glyphs, and the perceived area is the mean magnitude. Both methods of mapping uncertainty may be useful, as the length scaling emphasizes areas with higher uncertainty, and the area scaling gives a more perceptually accurate depiction of the current's magnitudes. Comparing Fig. 9 and Fig. 11 one may see which vectors have uncertain measurements, get a good indication of the flow, and have an accurate perception of the relative current magnitudes. It is also useful to compare Fig. 8 to Fig. 16 to contrast the overloading approach with the verity approach for the very same data.

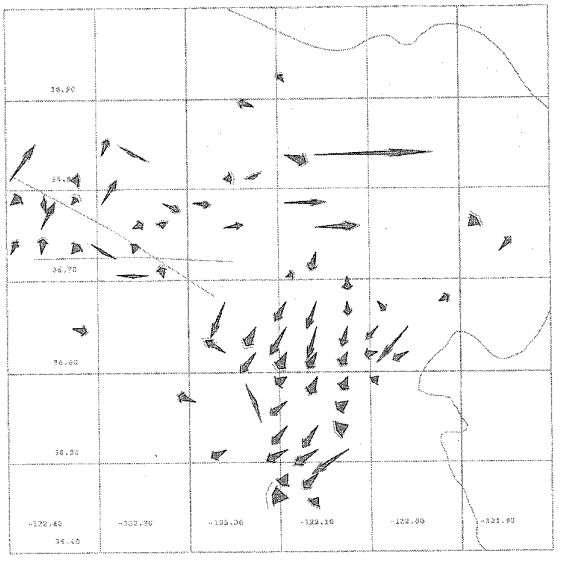

Fig. 11. Uncertainty glyphs, area scaled to magnitude, codar vector calculation Method I.

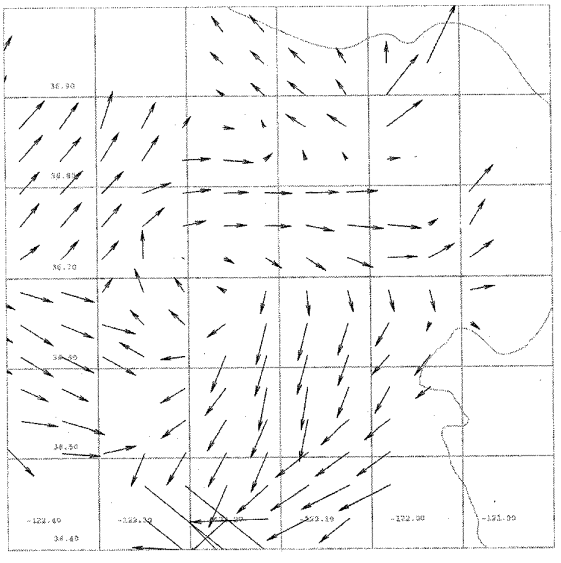

Fig. 12. Arrow glyphs, length scaled to magnitude, codar vector calculation Method II.

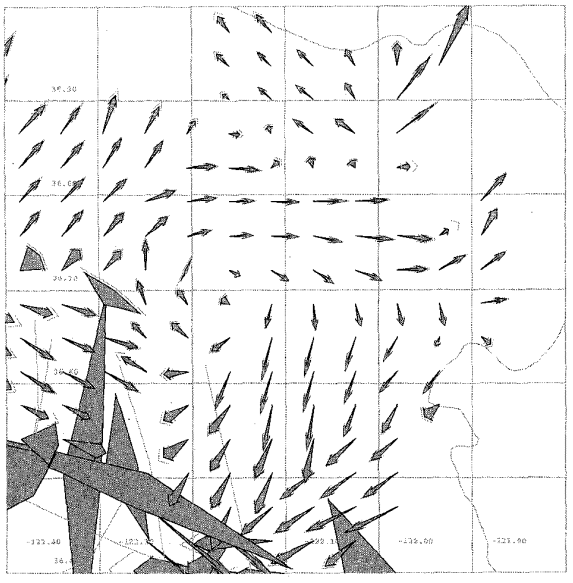

Fig. 13. Uncertainty glyphs, length scaled to magnitude, codar vector calculation Method II.

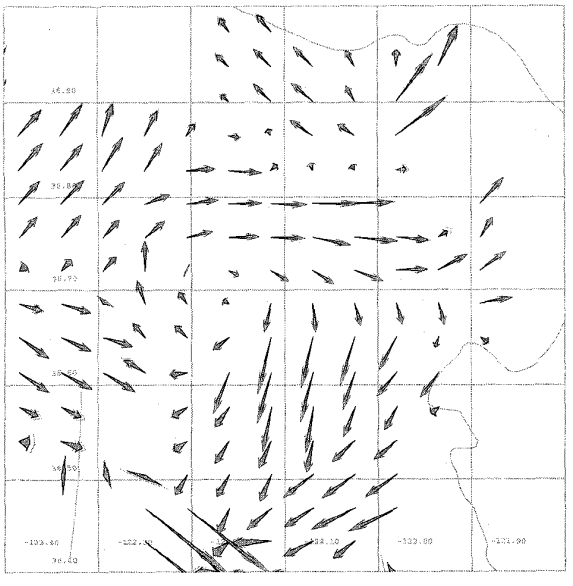

Fig. 14. Uncertainty glyphs, area scaled to magnitude, Codar vector calculation Method II.

EXAMPLE 3. *(Verity Visualization of Radar Sensed Winds)* The windprofiler data described in Section 2.3 and Figs. 2 and 3 can also be visualized with our uncertainty vectors showing the broad applicability of the glyph with real applications. The spectral data and signal power are used to compute uncertainty. Winds identified by strong radar returns are more accurate. Figs. 17, 18, and 19 show data collected from a NOAA wind profiler at Long Marine Laboratory installed as part of our REINAS system development. Fig. 17 shows wind barb glyphs; Fig. 18 shows uncertainty vector glyphs; and Fig. 19 shows arrow glyphs. Note that the uncertainty information is not available with the barbs or the arrows. The plots show winds at vertical heights in meters over different hours. As with the wind barbs, winds plotted have no vertical component, and represent only the horizontal direction with north to the top, east to the right, and south to the bottom.

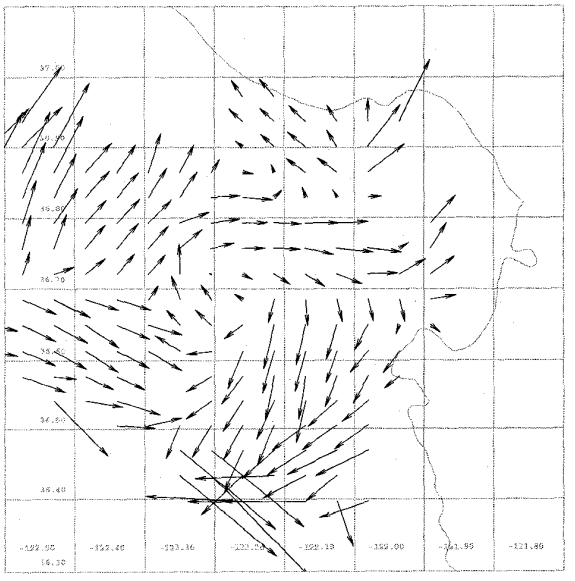

Fig. 15. Large version of Fig. 12, arrow glyphs, length scaled to magnitude, codar vector calculation Method II.

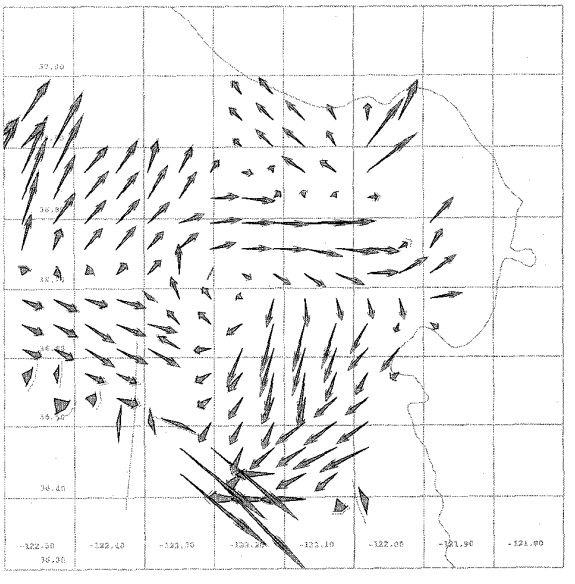

Fig. 16. Large version of Fig. 14, uncertainty glyphs, area scaled to magnitude, codar vector calculation Method II.

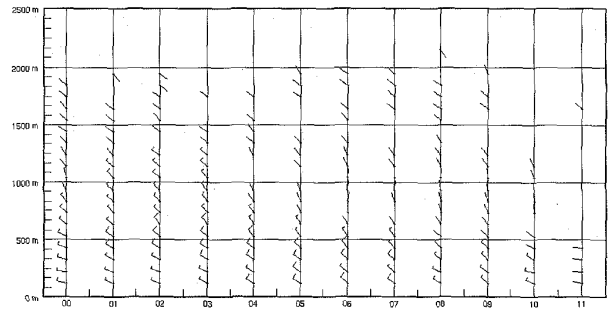

Fig. 17. Windprofiler winds using meteorological wind barb glyphs where the flag encodes the magnitude of wind/w and the flag points into the direction the wind is coming from.

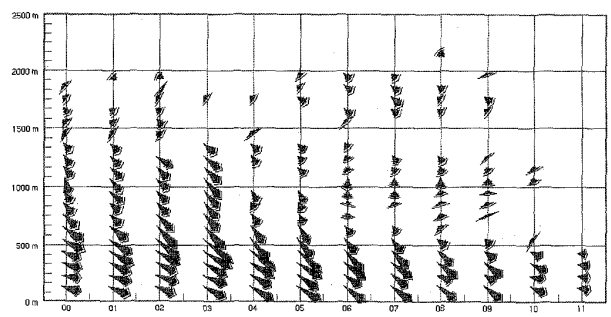

Fig. 18. Same windprofiler winds using uncertainty glyphs to visualize uncertainty derived from signal strength, magnitude mapped to area.

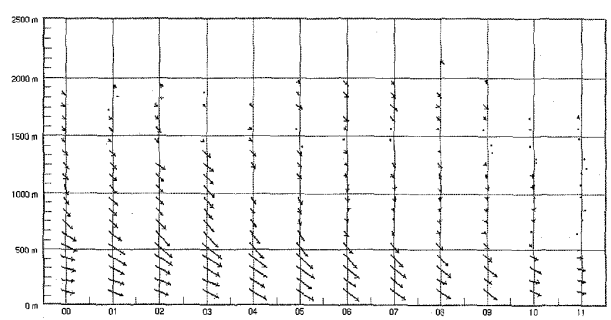

Fig. 19. Same windprofiler winds using arrow glyphs.

EXAMPLE 4. *(Verity Visualization of Interpolated Winds)* At meteorological stations, wind measurements are gathered at a one second sampling rate. To provide a denser field of winds we interpolate the sparse sampling of meteorological stations over the Monterey Bay. Figs. 20 and 21 show arrow glyphs and uncertainty glyphs where uncertainty is assumed to increase linearly with distance.

Fig. 3 shows how wind vectors are typically represented as wind barbs. Such a representation of hourly averaged winds, gives no indication of uncertainty which we know is present from the spectral data. In contrast, Fig. 21 shows wind vectors with uncertainty using uncertainty vector glyphs. The wind magnitude is mapped to the area of the glyph. Using this glyph, the uncertainty is apparent within each vector. The viewer cannot detach the uncertainty from the vector itself. This makes the data analysis simpler. In addition, in comparison with Fig. 20, we would argue that there is more information with a comparable amount of ink used, similar clutter, and a clearer understanding of the vector field.

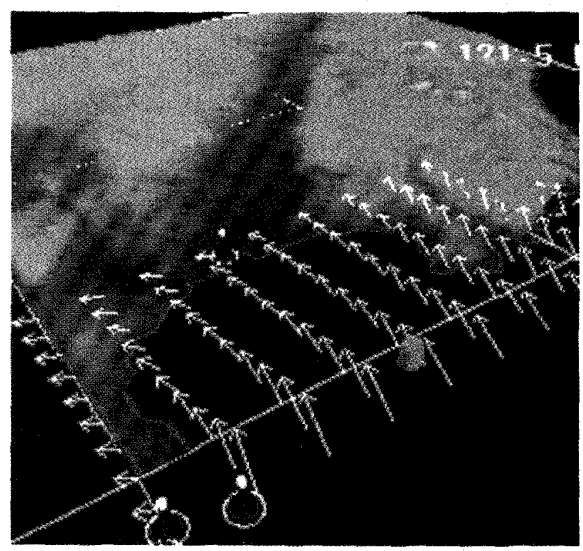

Fig. 20. Visualization of wind velocity without uncertainty. Measured surface wind vectors from buoys and meteorological stations are interpolated and resampled over the Monterey Bay reon. Regular arrow glyphs are used to represent the wind vectors

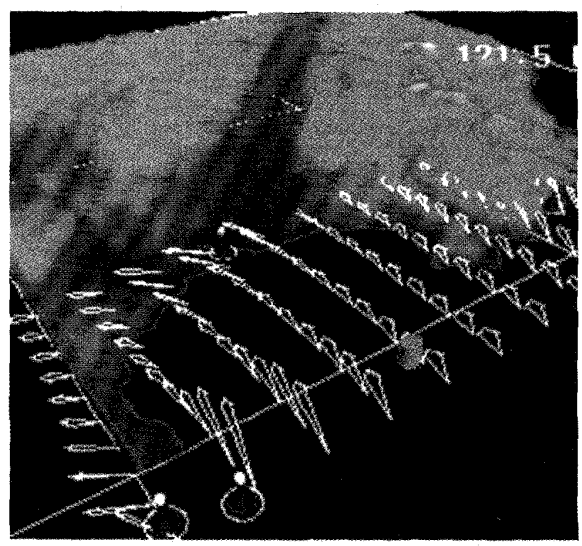

Fig. 21. Same vector data with uncertainty that increases with distance from sensor sites giving a different impression. The new glyph incorporates directional uncertainty in the angle between the edges of the glyph. The magnitude is mapped to the area.

4 EVALUATION

There are qualitative and quantitative methods to evaluate the effectiveness of any new visualization technique. We use both of these techniques. The quantitative approaches are less subjective and, therefore, simpler to use. There has been significant research on how to evaluate graphical per-

ception. Cleveland [5], [6] works with graphical specifiers, a length, area, angle, etc. Kosslyn [16] breaks the evaluation of a graphic into: 1) specifiers, 2) frameworks, 3) labels, and 4) background. Tufte [37], [38] presents qualitative evaluation methods such as: data-ink maximization, clutter or confusion minimization, moire pattern minimization, and multifunctional graphics elements. Carswell [2] uses hundreds of prior graphical perception studies to evaluate the effectiveness of Cleveland's specifiers methodology in predicting graph effectiveness over Tufte's data-ink maximization ratio. We briefly discuss some of the quantitative evaluation we used, then present results from our qualitative perceptual study. While only the most basic tasks were tested for, other tasks for the new glyphs are possible such as global comparisons and synthesis as well as freedom in choosing labels, backgrounds, etc.

4.1 Quantitative Evaluation

One reason for scaling the area of the glyph to the magnitude of the vector field, is that people perceive area over length [37]. Therefore, the perceived glyphs correlate to the true strength of the vector field. But, area is more error prone to decode than length so both variants may be useful. A side benefit of these glyphs is the fact that glyphs showing uncertainty, and those not showing uncertainty have exactly the same area. This gives us the same *ink* amount for plots of the same vector fields with each different glyph, arrow versus uncertainty glyph. The information content is greater however, because not only are we plotting *magnitude* and *bearing*, but we also include *bearing-deviation* without additional ink. Therefore, the data-to-ink ratio improvement is $(4/inkarea)$ to $(5/inkarea)$ for a 5/4 improvement (x location, y location, bearing, magnitude, and uncertainty bearing) for plotting our chosen glyph compared to an arrow glyph. When the magnitude uncertainty is also shown, there is a small increase in the amount of ink used for the upper deviation. The amount of increased ink usage is also analytically computable, but depends on the ratio $r_{a/b}$. In this case the *magnitude* and *bearing*, *deviation bearing*, and *deviation magnitude* are shown in the plot with slightly more ink for approximately a factor of 3/2 improvement in the quantitative data/ink maximization ratio. Note: that the data/ink ratio may or may not be a good indicator for glyph evaluation, but we provide it to assist other researchers in evaluation and comparison to our glyphs.

We have also done qualitative evaluations. Some of the qualitative metrics are clearly applied, others are not. We have taken advantage of collaborating organizations to gain access to professional meteorologists who helped evaluate our glyphs. We used decoding tests, where graphics with uncertainty glyphs and with arrow glyphs are evaluated to determine the interpretation accuracy.

4.2 Qualitative Experimental Methodology

We followed the approach of Cleveland, Kosslyn, and Carswell [2], [5], [6] by treating visualization as *visual decoding* of encoded information. We focused on the simplest aspect of the glyphs: Can users accurately decode information from the glyphs? A training session introduced the test subjects to the conventions used, such as degrees clockwise from north for angular judgments. We used test sections for arrow glyphs (Section 1.1), uncertainty glyphs (Section 1.2), fields of arrow glyphs (Section 2.1), and fields of uncertainty glyphs (Section 2.2). Section 1 of the test used a field of four glyphs, where one glyph was given as a reference, while Section 2 used fields of 170 to 300 glyphs. Section 1.1 had 24 questions; Section 1.2 had 48 questions; Section 2.1 had 32 questions; and Section 2.2 had 64 questions. For each question, test subjects were asked to fill in the magnitude, bearing, uncertainty magnitude, and/or uncertainty bearing. Our 12 test subjects were naval officers studying for their masters degrees in Meteorology at the Naval Postgraduate School, Monterey. They had professional training in the interpretation of visual graphics elements including vector fields. The test fields were similar to the codar vector plots in Figs. 9, 10, 11, 12, 13, 14, 15, and 16, and included synthetic and measured data. Test question response times were not collected.

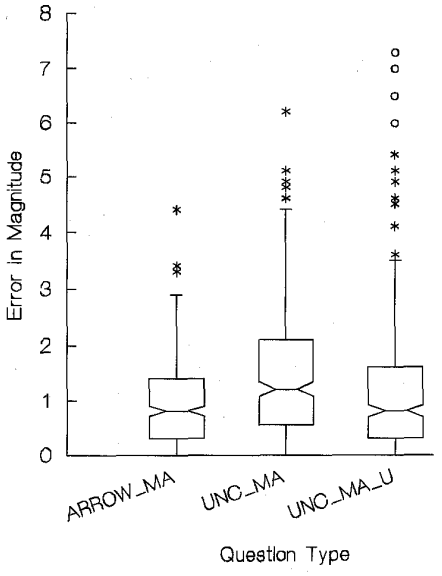

Fig. 22. Error in magnitude for all answers; left: ARROW_MA-arrow glyph; middle: UNC_MA-uncertainty glyph; right: UNC_MA_U-uncertainty glyph uncertainty.

The variance of the errors as calculated by

$$|answer - truevalue|,$$

as well as the means are shown in Figs. 22, 23, 24, and 25. Tukey box plots [39], plotted by Systat (TM), are used to show the variation in test responses. The box plots were chosen to present a large amount of information about the errors with economy. Box plots are defined in Tukey [39] and also in the Systat documentation. The central line of the box is the median value; the edges of the box are the hinges and denote the split between the range and the median. Whiskers, or the small thin lines, are drawn from the hinges to the extremes if they lie inside the fences. Inner and outer fences are defined as the hinge plus 1.5 times the interhinge range and the hinge plus three times the interhinge range. Values outside the inner fence are plotted with asterisks, and values outside the outer fence are plotted with circles.

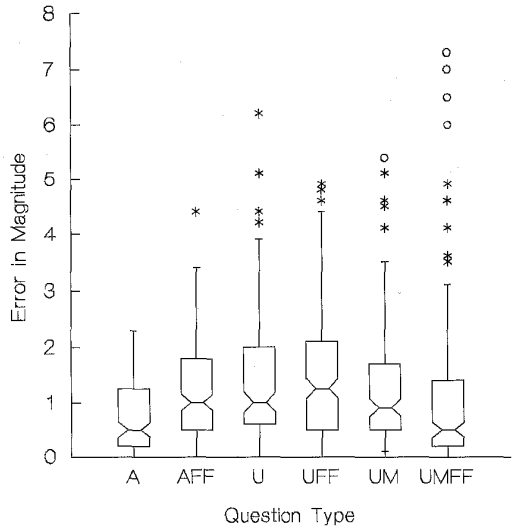

Fig. 23. Magnitude error Section 1 (4 vector field) and Section 2 (270–300 vector field or full field), from left to right, A-arrow glyph, AFF-arrow glyph full field, U-uncertainty glyph, UFF-uncertainty glyph full field, UM-uncertainty glyph uncertainty, UMFF-uncertainty glyph uncertainty full field.

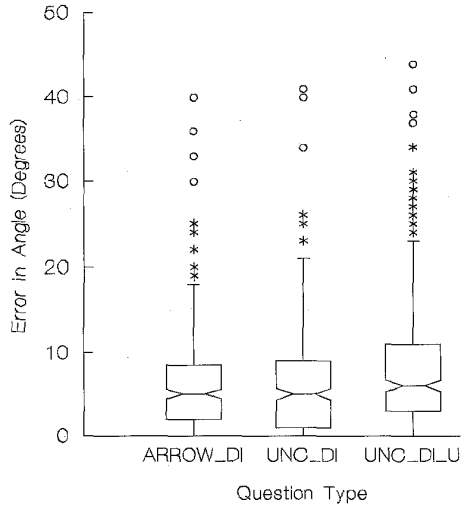

Fig. 24. Error in bearing for all answers; left: ARROW_DI-arrow glyph; middle: UNC_DI-uncertainty glyph; right: UNC_DI_U-uncertainty glyph uncertainty.

4.3 Qualitative Experimental Results

The experimental results provide a basis for our claims of the glyphs utility. Figs. 22, 23, and 24 show the errors for all answers and Figs. 23 and 25 break statistics out by test section. In the plots, the vertical scales are error in units-magnitude for Figs. 22 and 23 and error in degrees for Figs. 24 and 25. Glyph magnitudes varied from 1 to 10 units. The magnitude decoding was not as accurate as the bearing decoding as shown in Figs. 22 and 23. The mean errors and quartiles for all answers are given in Figs. 22 and 24 where ARROW stands for the arrow glyph, UNC for the uncertainty glyph, MA for magnitude, DI for direction, and U for the decoding of the uncertainty value. The mean errors are 0.989 arrow and 1.46 uncertainty glyph, while the standard deviations are 0.835 arrow and 1.18 uncertainty glyph. The glyph magnitudes varied from a scale of 1 to 10, so these errors are about 10%. The encoding of magnitude by area for the uncertainty glyph was not expected to be easy to decode, shown by studies by Cleveland [5], [6]. Decoding lengths is easier than areas, but the effect of high angular uncertainties was best counteracted by magnitude scaling, Figs. 11, 14, and 16.

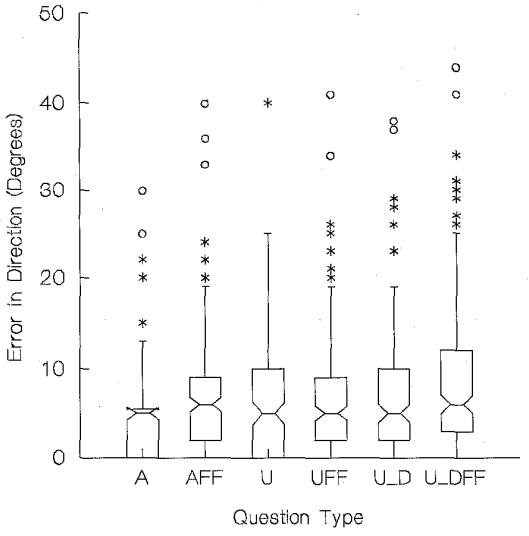

Fig. 25. Bearing error Section 1 (4 vector field) and Section 2 (270–300 vector field or full field), from left to right, A-arrow glyph, AFF-arrow glyph full field, U-uncertainty glyph, UFF-uncertainty glyph full field, U_D-uncertainty glyph uncertainty, U_DFF-uncertainty glyph uncertainty full field.

The angular error for the two glyphs is statistically equivalent (ARROW_DI vs UNC_DI Fig. 24), with a mean of 6.11 degrees for the arrow glyph and 6.23 degrees for the uncertainty glyph. The standard deviations are 6.01 degrees for the arrow glyph and 6.32 degrees for the uncertainty glyph. It is practical to assume one can only accurately resolve 5-degree angles in a 360 degree frame of reference, about 1% to 2% acuity. The conclusion of the mean errors is that the uncertainty glyph is, on the average, no worse than the arrow glyph for decoding bearing and perhaps statistically different, but not practically different for the magnitude.

In addition to bearing and magnitude, the uncertainty glyph presents two other quantities: bearing uncertainty and magnitude uncertainty whose experimental decoding errors are given in box plot UNC_MA_U and UNC_DI_U, Figs. 22 and 24 , and in the other figures as well. The angular uncertainty decoding error mean is 8.34 degrees and standard deviation is 8.02 degrees. The magnitude uncertainty decoding mean is 1.15 and the standard deviation is 1.26. Showing that the decoding errors for the uncertainties are comparable to those for the bearing and magnitude. These results were better than expected for the uncertainty, and illustrate that the uncertainty information can be quantitatively decoded from the glyphs.

In addition to the total summaries, breakdowns were done for the separate sections of the test. Recall Section 1 of the test used a field of four glyphs, while Section 2 used fields of 170 to 300 glyphs or full fields. The mean errors and quartiles for each section are given in Figs. 23 and 25, where FF stands for full field, so from the left there is A-arrow error, AFF-arrow full field, U-uncertainty glyph, UFF-uncertainty glyph full field, U(MD)-uncertainty glyph (magnitude/direction), U(MD)FF-uncertainty glyph (magnitude/direction) full field. The full field decoding is more error prone in all of the data but for the uncertainty magnitude. The difficulties for the full field are the higher density of glyphs, and the smaller size of the glyphs to fit them into a high density field. The effect of sparse field to dense field is similar for both the arrow glyph and the uncertainty glyph.

The statistical significance of our study is good for the directional error mean comparisons, where a t-test supports the hypothesis that the means of the errors are equal to 80% probability. We used a direct comparison of the 336 cases (all questions from all test subjects) of the arrow glyph to the uncertainty glyph using a paired t-test in Systat. Of course, having more data would provide more confidence. The magnitude coding is more difficult for both the arrows, and for the uncertainty glyphs, and the t-test does not support the hypothesis that the same errors are achieved. The test statistics also show that the uncertainty glyph magnitude error is higher than the error for the arrow glyphs as shown in Fig. 22. The statistical significance is also not relevant if the data does not have practical significance, but as stated earlier the errors are within practical limits for the ability to resolve angles and lengths. Strong statistical significance does not prove practical significance which is why we have presented the distribution of variances as used by Carswell and commented on the expected accuracy of the decoding. The cause for the difficulty in comparing the magnitude decoding error for the arrow and uncertainty glyph is most likely a direct result of the different encoding used for each, length versus area—a hypothesis supported by Cleveland and Carswell. Caution must also be used because of our specialized test subjects, who have knowledge of how to decode glyphs. But, we felt that the utility of the glyph should be tested by those who would actually use it.

The study shows that the uncertainty glyphs can be decoded with error similar to the arrow glyphs; that the uncertainty can be decoded from the glyphs with error similar to the bearing and magnitude error; that decoding area is more error prone than decoding length, confirming Cleveland's results; and that sparse fields versus dense fields has an effect for both glyphs, of a similar magnitude. From all of these results, we conclude that the experiments show the uncertainty glyph effectively encodes bearing, magnitude, uncertainty bearing, and uncertainty magnitude. It may very well be that an alternative glyph is superior in encoding and decoding of four values, but the experimental results provide a base line for comparison of future glyphs.

5 Summary and Conclusions

Scientific data from instruments, numerical models, or interpolation schemes almost invariably contain some degree of error or uncertainty. Display of such scientific data without uncertainty information is incomplete and may lead to erroneous conclusions. Visualization of data with uncertainty information allows more accurate and effective interpretation.

In this paper, we showed scientific data collected from different sources, derived uncertainty information, and presented some ideas on designing uncertainty vector glyphs. We defined visualization overloading and verity visualization, illustrating how our new glyphs represent the latter. In our research on verity visualization, we have seen that it is unambiguous as compared to other approaches, but it is not possible for all data visualization techniques. We showed examples of vector field visualizations with uncertainty for ocean current data, vertical wind profiler data, and interpolated wind data. We also showed qualitative and quantitative evaluations of our new visualizations. Our perceptual experiment showed that the decoding of the uncertainty specifiers is accurate, and that the decoding error of the vectors bearing and magnitude is on the order of the decoding error of traditional arrow glyphs. The error for both glyphs was experimentally 6 degrees in bearing and 10% in magnitude. This means that the uncertainty glyphs are a substantial improvement as they provide more information, that is accurately decodable, than traditional glyphs. Since no single technique of visualization works the best for all data and applications, experiments are still needed to identify effective visualization strategies that work well in a given context. We have shown, however, that visualization with the uncertainty glyphs proves quite valuable when data analysts are looking into the validity of their data. We believe our glyphs are superior, and will come into more common use because of their ease of understanding and information presentation.

Acknowledgments

We thank Dr. Daniel Fernandez for his extensive help, and advice on uncertainty in ocean current vectors. We thank Professor Wendell Nuss and Dr. Paul Hirschberg for their-support in providing Naval Research Laboratory's NORAPS output data from the Naval Postgraduate School. We especially thank the students who programmed some of thevisualizations including Dr. Naim Alper, Elijah Saxon, Jeff Furman, Michael Clifton, Steve Hodges, and Alan Tifford. And we also thank all of those involved on the REINAS project. This project is supported by the Office of Naval Research under Grant No. N00014-92-J-1807 and the National Science Foundation under Grant No. IRI-9423881. Some of the material presented in this paper appeared as "Glyphs for Visualizing Uncertainty in Environmental Vector Fields," C.M. Wittenbrink et al. [43].

REFERENCES

[1] M.K. Beard, B.P. Buttenfield, and S.B. Clapham, "NCGIA Research Initiative 7: Visualization of Spatial Data Quality," Technical Paper 91-26, Nat'l Center for Geographic Information and Analysis, Oct. 1991.

[2] C.M. Carswell, "Choosing Specifiers: An Evaluation of the Basic Tasks Model of Graphical Perception," *Human Factors*, vol. 34, no. 5, pp. 535–554, Oct. 1992.

[3] R. Clancy, J. Harding, K. Pollak, and P. May, "Quantification of Improvements in an Operational Global-Scale Ocean Thermal Analysis System," *J. Atmospheric and Oceanic Technology*, vol. 9, no. 1, pp. 55–66, 1992.

[4] D. Clark and F. Wilson, "An Automated Method for Low Level Wind Shear Alert System (LLWAS) Data Quality Analysis," Tech. Report ATC-207, MIT Lincoln Laboratory, Lexington, Mass., May 1994.

[5] W.S. Cleveland, *The Elements of Graphing Data*. Wadsworth, 1985.

[6] W.S. Cleveland and R. McGill, "An Experiment in Graphical Perception," *Int'l J. Man-Machine Studies*, vol. 25, no. 5, pp. 491–500, Nov. 1986.

[7] E. Cluff, R. Burton, and W. Barrett, "A Survey and Characterization of Multidimensional Presentation Techniques," *J. Imaging Technology*, vol. 17, no. 4, 1991.

[8] W.C. deLeeuw and J.J. van Wijk, "A Probe for Local Flow Field Visualization," *Proc. Visualization '93*, pp. 39–45, IEEE CS Press, Oct. 1993.

[9] G.Dutton, "Handling Positional Uncertainty in Spatial Databases," *Proc. Fifth Int'l Symp. Spatial Data Handling*, pp. 460–469. Univ. of So. Carolina, Aug. 1992.

[10] P. Fisher, "First Experiments in Viewshed Uncertainty: The Accuracy of the Viewshed Area," *Photogrammetric Engineering and Remote Sensing*, vol. 5, no. 10, pp. 1,321–1,327, 1991.

[11] P. Fisher, *Visualization in Geographical Information Systems*, chapter on Animation and Sound for the Visualization of Uncertain Spatial Information, pp. 181–185, 1994.

[12] N.D. Gershon, "Visualization of Fuzzy Data Using Generalized Animation," *Proc. Visualization '92*, pp. 268–273, IEEE CS Press, Oct. 1992.

[13] M. Goodchild, B. Buttenfield, and J. Wood, *Visualization in Geographical Information Systems*, chapter on Introduction to Visualizing Data Validity, pp. 141–149, 1994.

[14] R.M. Hodur, "Evaluation of a Regional Model with an Update Cycle," *Monthly Weather Review*, vol. 115, no. 11, pp. 2,707–2,718, Nov. 1987.

[15] G. Hunter and M. Goodchild, "Managing Uncertainty in Spatial Databases: Putting Theory into Practice," *URISA J.*, vol. 5, no. 2, pp. 55–62, 1993.

[16] S. Kosslyn, "Understanding Charts and Graphs," *Applied Cognitive Psychology*, vol. 3, pp. 185–226, 1989.

[17] D. Law, "Effects of Precipitation, Convection, and Waves on NOAA Network Profilers," *Proc. 25th Int'l Conf. Radar Meteorology*, pp. 43–46, Am. Meteorological Soc., Boston, June 1991.

[18] Y. Leung et al., "Visualization of Fuzzy Scenes and Probability Fields," *Proc. Fifth Int'l Symp. Spatial Data Handling*, pp. 480–490. Univ. of So. Carolina, Aug. 1992.

[19] L.K. Lewis, J.M. Wilczak, A.B. White, and L. Zhang, "Newly Developed X–Windows Tools for Analyzing the Boundary-Layer Structure," Technical Report, Environmental Technology Laboratory—NOAA, National Oceanic and Atmospheric Administration, Boulder, Col., Apr. 1994.

[20] B.J. Lipa and D.E. Barrick, "Least-Squares Methods for the Extraction of Surface Currents from Codar Crossed-Loop Data: Application at ARSLOE," *IEEE J. Oceanic Engineering*, vol. 8, no. 4, pp. 226–253, Oct. 1983.

[21] D. Long, P. Mantey, C.M. Wittenbrink, T. Haining, and B. Montague, "REINAS the Real-Time Environmental Information Network and Analysis System," *Proc. COMPCON*, pp. 482–487, San Francisco, IEEE, Mar. 1995.

[22] P. Mantey et al., "REINAS: Real-Time Environmental Information Network and Analysis System: Phase III—Systems Design," Tech. Report UCSC-CRL-94-08, CE and CS Boards, Univ. of California, Santa Cruz, 1994.

[23] G.L. Mellor, "User's Guide for a Three-Dimensional, Primitive Equation, Numerical Ocean Model," Tech. Report, Princeton Univ., 1993.

[24] H. Moellering, "The Proposed Standard for Digital Cartographic Data: Report of the Digital Cartographic Data Standards Task Force," *The American Cartographer*, vol. 15, no. 1, 1988.

[25] M. Monmonier, "Strategies for the Interactive Exploration of Geographic Correlation," *Proc. Fourth Int'l Symp. Spatial Data Handling*, vol. 1, pp. 512–521. IGU, July 1990.

[26] M. Monmonier, "Time and Motion as Strategic Variables in the Analysis and Communication of Correlation," *Proc. Fifth Int'l Symp. Spatial Data Handling*, pp. 72–81. Univ. of So. Carolina, Aug. 1992.

[27] A. Pang, "Spray Rendering," *IEEE Computer Graphics and Applications*, vol. 14, no. 5, pp. 57–63, 1994.

[28] A. Pang and N. Alper, "Bump Mapped Vector Fields," *Proc. SPIE & IS&T Conf. Electronic Imaging, vol. 2410: Visual Data Exploration and Analysis II*, pp. 78–86, color plate p. 205. SPIE, Feb. 1995.

[29] A. Pang, J. Furman, and W. Nuss, "Data Quality Issues in Visualization," *SPIE vol. 2178 Visual Data Exploration and Analysis*, pp. 12–23. SPIE, Feb. 1994.

[30] J.K. Petersen, "Map Processors," *GIS/LIS '89*, pp. 134–142. Am. Congress on Surveying & Mapping, Nov. 1989.

[31] R.M. Pickett and G.G. Grinstein, "Iconographic Displays for Visualizing Multidimensional Data," *Proc. Int'l Conf. Systems, Man, and Cybernetics*, pp. 514–519, IEEE, 1988.

[32] F.H. Post, "Glyph Versus Icon Terminology," personal communication, Nov. 1995. Prof. Post has spent some time considering the terminology, and decided that both are fine, while they prefer to use iconic, because they have low density displays—large glyphs/icons that are few in number. He also stressed the terminology of small icons for high density and large icons for low density.

[33] F.J. Post, T. van Walsum, F.H. Post, and D. Silver, "Iconic Techniques for Feature Visualization," *Proc. Visualization '95*, pp. 288–295, Atlanta, Ga., IEEE, Nov. 1995..

[34] W. Ribarsky, E. Ayers, J. Eble, and S. Mukherjea, "Glyphmaker: Creating Customized Visualizations of Complex Data," *Computer*, vol. 27, no. 7, pp. 57–64, 1994.

[35] S. Smith, R.D. Bergeron, and G.G. Grinstein, "Stereophonic and Surface Sound Generation for Exploratory Data Analysis," *Proc. CHI '90 Conf.*, pp. 125–132, ACM, 1990.

[36] B.N. Taylor and C.E. Kuyatt, "Guidelines for Evaluating and Expressing the Uncertainty of NIST Measurement Results. Tech. Report, Nat'l Inst. of Standards and Technology Technical Note 1297, Gaithersburg, Md., Jan. 1993.

[37] E.R. Tufte, *The Visual Display of Quantitative Information*. Graphics Press, 1983.

[38] E.R. Tufte, *Envisioning Information*. Graphics Press, 1990.

[39] J.W. Tukey, *Exploratory Data Analysis*. Addison-Wesley, 1977.

[40] J.Wilczak et al., "Contamination of Wind Profiler Data by Migrating Birds: Characteristics of Corrupted Data and Potential Solutions. Tech. Report, Environmental Technology Laboratory–NOAA, 1994.

[41] G.Wills et al., "Statistical Exploration of Spatial Data," *Proc. Fourth Int'l Symp. Spatial Data Handling*, vol. 1, pp. 491–500. IGU, July 1990.

[42] C.M. Wittenbrink, "Designing Optimal Parallel Volume Rendering Algorithms," PhD thesis, Univ. of Washington, 1993.

[43] C.M. Wittenbrink, E. Saxon, J.J. Furman, A.T. Pang, and S. Lodha, "Glyphs for Visualizing Uncertainty in Environmental Vector Fields," *vol. 2410, Proc. PIE & IS&T Conf., Electronic Imaging: Visual Data Exploration and Analysis*, pp. 87–100. SPIE, Feb. 1995.

Craig M. Wittenbrink (S'85–M'87–S'88–S'90–M'93) is a postdoctoral researcher at the University of California, Santa Cruz, where he does research in environmental visualization. He received the BS degree in electrical engineering and computer science from the University of Colorado in 1987, and the MS and PhD degrees in 1990 and 1993, respectively, both in electrical engineering, from the University of Washington. He was a design engineer with Boeing Aerospace from 1987 to 1989, where he developed computer image generators. He was a co-chair of the 1995 IEEE/ACM Parallel Rendering Symposium and is widely published in parallel-image, visualization, and graphics processing. He is a member of ACM, Siggraph, and the IEEE Computer Society.
http://www.cse.ucsc.edu/~craig.

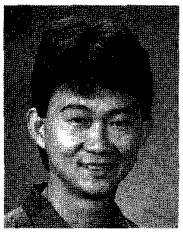

Alex T. Pang (S'87–M'91) obtained the BS degree in industrial engineering from the University of the Philippines and received the MS and PhD degrees in computer science from the University of California, Los Angeles, in 1984 and 1990, respectively. Dr. Pang is an assistant professor in the Computer and Information Sciences Board at the University of California, Santa Cruz. His current research interests are in computer graphics, scientific visualization, collaboration software, multimedia, and virtual reality interfaces.
http://www.cse.ucsc.edu/~pang.

Suresh K. Lodha (S'91–S'92–M'95) received an MSc degree in mathematics integrated with engineering from the Indian Institute of Technology, Kanpur, in 1976. He received an MS degree in mathematics from the University of California, Berkeley, in 1984 and a PhD degree in computer science from Rice University, Houston, in 1992. He is currently an assistant professor of computer science at the University of California, Santa Cruz. His research interests include geometric modeling, computer graphics, and scientific visualization.
http://www.cse.ucsc.edu/~lodha